

In-Hospital Stroke Prediction from PPG-Derived Hemodynamic Features

Jiaming Liu

Nanjing University of Aeronautics
and Astronautics
Nanjing, Jiangsu, China
gaming@nuaa.edu.cn

Cheng Ding*

Nanjing University of Aeronautics
and Astronautics
Nanjing, Jiangsu, China
chengding@nuaa.edu.cn

Daoqiang Zhang

Nanjing University of Aeronautics
and Astronautics
Nanjing, Jiangsu, China
dqzhang@nuaa.edu.cn

Abstract

The absence of pre-hospital physiological data in standard clinical datasets fundamentally constrains the early prediction of stroke, as patients typically present only after stroke has occurred, leaving the predictive value of continuous monitoring signals such as photoplethysmography (PPG) unvalidated. In this work, we overcome this limitation by focusing on a rare but clinically critical cohort—patients who suffered stroke during hospitalization while already under continuous monitoring—thereby enabling the first large-scale analysis of pre-stroke PPG waveforms aligned to verified onset times. Using MIMIC-III and MC-MED, we develop an LLM-assisted data mining pipeline to extract precise in-hospital stroke onset timestamps from unstructured clinical notes, followed by physician validation, identifying 176 patients (MIMIC) and 158 patients (MC-MED) with high-quality synchronized pre-onset PPG data, respectively. We then extract hemodynamic features from PPG and employ a ResNet-1D model to predict impending stroke across multiple early-warning horizons. The model achieves F1-scores of 0.7956, 0.8759, and 0.9406 at 4, 5, and 6 hours prior to onset on MIMIC-III, and, without re-tuning, reaches 0.9256, 0.9595, and 0.9888 on MC-MED for the same horizons. These results provide the first empirical evidence from real-world clinical data that PPG contains predictive signatures of stroke several hours before onset, demonstrating that passively acquired physiological signals can support reliable early warning, supporting a shift from post-event stroke recognition to proactive, physiology-based surveillance that may materially improve patient outcomes in routine clinical care.

Keywords

PPG, In-Hospital Stroke Prediction, Early Warning Systems

ACM Reference Format:

Jiaming Liu, Cheng Ding, and Daoqiang Zhang. 2026. In-Hospital Stroke Prediction from PPG-Derived Hemodynamic Features. In *Proceedings of the 32nd ACM SIGKDD Conference on Knowledge Discovery and Data Mining (KDD '26)*. ACM, New York, NY, USA, 11 pages.

1 Introduction

Stroke is a catastrophic vascular event that demands immediate intervention[11, 31]. While the clinical community has long sought methods for early prediction, progress has been severely limited by a fundamental data paradox: patients typically present to the hospital only post-onset[47]. Consequently, standard clinical datasets

contain abundant post-stroke data but suffer from a complete absence of pre-stroke physiological signals[21]. This "blind spot" has precluded the validation of continuous monitoring technologies, such as Photoplethysmography (PPG), for effective stroke prediction prior to onset[22].

From a biomedical engineering perspective, PPG is theoretically an ideal candidate for this task[61]. Stroke is driven by cerebrovascular hemodynamics—specifically, abrupt changes in vascular resistance and blood flow dynamics[43]. As PPG passively measures peripheral blood volume changes, it offers a direct window into the systemic cardiovascular state. However, the efficacy of PPG for stroke prediction remains an unproven hypothesis[56, 59], primarily attributable to the historical paucity of data documenting the physiological transition from a baseline state to an acute stroke event[7, 8, 26].

In this work, we overcome this barrier by targeting a unique and challenging cohort: in-hospital stroke patients. These are patients who were already under continuous physiological monitoring for other conditions when they suffered a stroke. This rare scenario offers a unique opportunity to capture "pre-stroke" waveform data unavailable in standard admission records. By retrospectively analyzing these cases, we can—for the first time—explore the feasibility of PPG-based early warning systems using real-world clinical data.

To operationalize this, we utilized two large-scale datasets, MIMIC-III [40] and MC-MED [29]. However, identifying these rare cases presents a significant mining challenge. The timestamps available in structured EHR data represent documentation time rather than the physiological onset of stroke, and therefore cannot be directly interpreted as onset time. To address this, we developed a pipeline using Gemini 3 Pro to extract exact onset timestamps from unstructured clinical notes, which were subsequently validated by physicians. This rigorous process allowed us to identify 176 patients in MIMIC-III and 158 patients in MC-MED who possess high-quality, synchronized PPG waveforms leading up to the event.

With this unprecedented data, we developed a deep learning framework to test our hypothesis. Hemodynamic features extracted from pre-onset PPG signals were fed into a ResNet-1D model to identify predictive signatures[23, 50, 55]. Across three early-warning horizons, the model demonstrates progressively improved performance. When trained and validated on the internal MIMIC-III cohort, F1-scores increase from 0.7956 at 4 hours to 0.8759 ± 0.0105 at 5 hours and 0.9406 at 6 hours prior to onset. Using the same trained model without any re-tuning, external evaluation on the MC-MED cohort yields F1-scores of 0.9256, 0.9595, and 0.9888 for the corresponding horizons. These results confirm the validity of PPG as a predictive signal for early stroke warning and demonstrate that temporally aligned, passively acquired physiological data can

*Corresponding Author

support reliable prediction with substantial lead time, beyond what is achievable through model-centric optimization alone.

2 Related Work

2.1 Stroke Prediction with EHR and ML

Traditional stroke stratification has evolved from rule-based scoring (e.g., Framingham) to high-dimensional modeling using EHR[1, 2, 12, 41, 54]. While early ML approaches (e.g., Random Forests, SVMs) effectively leveraged structured features like demographics and diagnosis codes for population-level risk assessment [10, 20, 24, 25, 34, 37, 46, 49, 52, 60], they rely on static snapshots.

These methods inherently lack the temporal granularity required for acute, real-time physiological monitoring in clinical settings.

2.2 Occult Disease Detection via Physio-Signals

Addressing EHR limitations, Deep Learning (DL) architectures now enable the identification of occult disease signatures from continuous physiological signals, even absent explicit pathological events [5, 30, 39, 58]. A key area is extracting risk precursors from Normal Sinus Rhythm in ECGs [28, 32, 45, 65]. Notably, Gadaleta et al. [16] demonstrated that sub-clinical morphological features in AF-free intervals could accurately quantify near-term Atrial Fibrillation risk. These findings validate the hypothesis that DL can extract latent morphological biomarkers invisible to standard clinical interpretation [13, 18, 48, 53].

2.3 PPG Hemodynamics and the Label Gap

PPG offers a complementary window into cerebrovascular hemodynamics, reflecting vascular stiffness and aging [6, 9, 14, 38, 44]. While recent end-to-end DL models successfully infer indirect stroke factors (e.g., cuffless blood pressure, AF) from raw pulse waves [35, 42, 62], the direct prediction of *acute in-hospital stroke* remains unexplored [3]. Existing PPG research is predominantly retrospective or associative [33, 64], lacking predictive capability for the critical pre-onset window.

This gap stems not from sensor limitations, but from a fundamental "label unavailability" challenge: the scarcity of in-hospital stroke datasets prevents the construction of aligned pre-stroke windows for supervised learning [4, 51]. Our work addresses this bottleneck by establishing a reliable temporal reference via an LLM-enhanced waveform anchoring method, enabling the first data-centric exploration of PPG-based acute stroke prediction [57].

3 Methods

To validate the predictive value of continuous physiological monitoring for impending stroke, this work utilizes two large-scale critical care databases: MIMIC-III [40] as the internal development set and MC-MED [29] for external evaluation. The core methodological challenge addressed in this work is the absence of structured timestamps for in-hospital stroke onset in standard EHR. To overcome this, this work establishes a comprehensive data processing pipeline, as illustrated in Fig. 1, consisting of three primary stages: (1) Cohort Identification and Temporal Anchoring, where we combine ICD-based screening with an LLM-assisted extraction workflow to pinpoint precise stroke onset timestamps from unstructured clinical

narratives; (2) Physiological Signal Preprocessing, involving the extraction, quality assessment, and windowing of high-frequency PPG waveforms aligned to the validated onset times; and (3) Deep Learning Modeling, employing a ResNet-1D architecture to capture hemodynamic precursors across varying prediction horizons.

3.1 Data Source

This study leverages two distinct large-scale clinical databases to ensure both robust model development and external generalizability: the MIMIC-III [40] and the MC-MED [29].

MIMIC-III (Internal Cohort): Sourced from the Beth Israel Deaconess Medical Center in Boston, MA, this single-center database serves as our primary training and internal validation environment. It comprises comprehensive de-identified health-related data associated with over 40,000 patients who stayed in critical care units between 2001 and 2012. Our analysis focused on the subset of 38,548 patients for whom sufficient waveform data was potentially retrievable. Within this population, the identified stroke subset exhibited a mean age of 66.9 years (SD 15.3), notably higher than the overall cohort mean of 63.8 years. Racial demographics within the stroke subset largely mirrored the general MIMIC population, with 124 (70.5%) identified as White, 13 (7.4%) as Black or African American, and 5 (2.8%) as Asian. Comorbidity profiles indicated significantly higher rates of hypertension in the stroke group (76.7% vs. 56.8%) and hyperlipidemia (39.8% vs. 31.8%), consistent with established vascular risk factors.

MC-MED (External Cohort): To rigorously test model transferability, we employed MC-MED, a large-scale multi-center database aggregating EHR and physiological data from diverse hospital systems across the West Coast. This dataset provides a substantially larger general pool of 118,385 patients. The confirmed stroke subset in MC-MED presented a distinct demographic profile compared to MIMIC-III, with a higher mean age of 71.2 years (SD 15.0) versus the general MC-MED population of 53.3 years. The racial composition of the stroke subset in MC-MED differed from the internal set, with a larger proportion of Asian patients (45 individuals, 28.5%) compared to White (74 individuals, 46.8%) and Black or African American patients (8 individuals, 5.1%).

As summarized in Table 1, both stroke subsets consistently skewed older and demonstrated a higher burden of vascular comorbidities relative to their respective general populations, reinforcing the clinical validity of the extracted cohorts despite the heterogeneity in data sources.

3.2 Stroke Onset Time Extraction via LLM

The main obstacle to training supervised models for acute in-hospital stroke lies in the insufficient temporal resolution of the standard EHR. While structured data fields reliably identify the occurrence of a stroke, they inherently lack the granularity to pinpoint the precise moment of symptom onset—a critical variable for defining the pre-event window. Consequently, the crucial timestamp that marks the physiological transition from baseline to pathology is typically embedded within unstructured free-text clinical narratives.

To bridge this gap efficiently, we implemented an automated NLP pipeline to parse unstructured clinical narratives from MIMIC-III and MC-MED datasets. To ensure high-fidelity anchoring, the

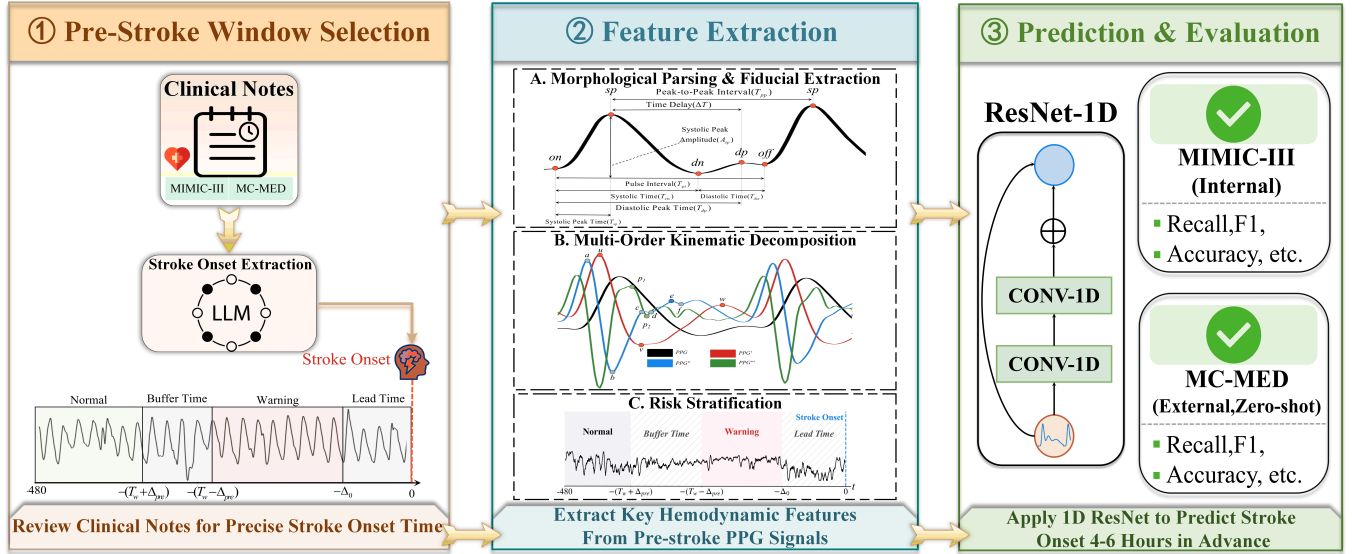


Figure 1: Overview of the proposed framework. The pipeline comprises three phases: (1) Temporal Anchoring: LLM-driven extraction of precise stroke onset timestamps from unstructured clinical notes; (2) Feature Engineering: Derivation of hemodynamic biomarkers from PPG waveforms and their derivatives; and (3) Predictive Modeling: A ResNet-1D network for early stroke warning, validated on internal (MIMIC-III) and external (MC-MED) cohorts.

pipeline enforces a hierarchical temporal extraction strategy across both cohorts. First, it prioritizes *Explicit Semantic Alignment*, scanning for direct temporal markers (e.g., "onset at 6:30 AM") and resolving relative expressions against the note's metadata to derive an absolute timestamp. In the absence of a specific onset description, the system utilizes an *Implicit Temporal Proxy* if an acute event is confirmed, defaulting to the note's creation time as a conservative upper bound. Conversely, records describing unrelated pathologies or historical strokes without acute recurrence are flagged as non-events and excluded.

This logic converts unstructured clinical notes into structured temporal indices. We validated this method via a protocol involving two neurologists. On a stratified subset of 100 cases, the model achieved 95.0% concordance within a ± 15 -minute tolerance of the ground truth. This tolerance aligns with the labeling strategy detailed in Section 3.4, which defines the normal, warning, and buffer zones for stroke prediction.

3.3 Hemodynamic Feature Engineering

Based on the verified stroke onset timestamps, we implemented a pipeline to derive standardized predictors of acute cerebrovascular events. Utilizing the pyPPG toolbox [19], we extracted 74 morphological biomarkers per cardiac cycle from the raw PPG signal and its derivatives to capture hemodynamic dynamics. Recognizing the limitations of absolute physiological measurements due to inter-patient heterogeneity, we applied a normalization technique to isolate pathological trajectories. Each metric $x(t)$ was projected into a relative deviation space to quantify the magnitude of divergence. Consequently, a Relative Displacement score (\mathcal{F}_{rel}) was calculated relative to a subject-specific baseline μ_{base} , established as the mean value during the initial stable period:

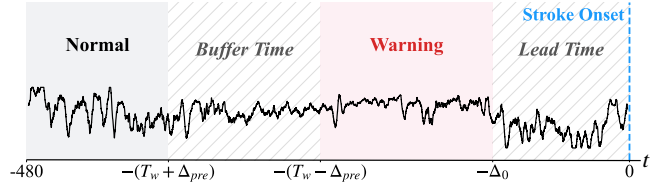


Figure 2: Temporal Labeling Strategy. Timeline aligned to stroke onset ($t = 0$) with exclusion buffers to mitigate label noise and prevent leakage.

$$\mathcal{F}_{rel}(t) = \frac{x(t) - \mu_{base}}{|\mu_{base}|} \quad (1)$$

This transformation doubles the feature space, capturing both instantaneous systemic states and temporal deviations from homeostasis.

3.4 Temporal Labeling Strategy

The integrity of these longitudinal signals was preserved via a rigorous, source-isolated preprocessing protocol. Because the raw datasets aggregate heterogeneous recording sessions characterized by natural discontinuities (e.g., device re-attachments), we restricted all artifact remediation and imputation operations to the boundaries of individual source files. This constraint precluded the artificial synthesis of temporal continuity between unrelated physiological states. Following this source-specific standardization, the high-dimensional feature space was distilled into a refined set of robust stroke precursors through a two-stage statistical filtering process. We first evaluated the discriminative capacity of each feature

Table 1: Baseline characteristics of the internal (MIMIC) and external (MC-MED) cohorts. Continuous variables are reported as mean (SD) and median [IQR]; categorical variables are reported as n (%).

Characteristic	Subgroup	MIMIC (Internal)		MC-MED (External)	
		Overall	Stroke subset	Overall	Stroke subset
Sample size (N)	Overall / Stroke	38,548	176	118,385	158
Age, years	Mean (SD)	63.8 (17.5)	66.9 (15.3)	53.3 (20.4)	71.2 (15.0)
	Median [IQR]	65.7 [52.4–77.9]	68.8 [54.2–79.6]	53.0 [35.0–70.0]	75.0 [61.0–83.0]
Age group	< 65 years	18,769 (48.7%)	76 (43.2%)	79,429 (67.1%)	48 (30.4%)
	≥ 65 years	19,779 (51.3%)	100 (56.8%)	38,956 (32.9%)	110 (69.6%)
Age group	18–39 years	4,075 (10.6%)	9 (5.1%)	36,814 (31.1%)	4 (2.5%)
	40–59 years	10,833 (28.1%)	52 (29.5%)	33,345 (28.2%)	31 (19.6%)
	60–79 years	15,775 (40.9%)	75 (42.6%)	33,434 (28.2%)	71 (44.9%)
	≥ 80 years	7,865 (20.4%)	40 (22.7%)	14,792 (12.5%)	52 (32.9%)
Sex	Female	16,732 (43.4%)	88 (50.0%)	64,272 (54.3%)	76 (48.1%)
	Male	21,816 (56.6%)	88 (50.0%)	54,077 (45.7%)	82 (51.9%)
	Unknown	0 (0.0%)	0 (0.0%)	36 (0.0%)	0 (0.0%)
Race	White	27,477 (71.3%)	124 (70.5%)	47,504 (40.1%)	74 (46.8%)
	Asian	911 (2.4%)	5 (2.8%)	19,430 (16.4%)	45 (28.5%)
	Black or African American	2,943 (7.6%)	13 (7.4%)	7,653 (6.5%)	8 (5.1%)
	Pacific Islander	11 (0.0%)	0 (0.0%)	2,468 (2.1%)	2 (1.3%)
	American Indian/Alaska Native	20 (0.1%)	0 (0.0%)	309 (0.3%)	0 (0.0%)
	Other	2,294 (6.0%)	21 (11.9%)	39,951 (33.7%)	28 (17.7%)
	Declines to state	0 (0.0%)	0 (0.0%)	551 (0.5%)	0 (0.0%)
	Unknown	4,892 (12.7%)	13 (7.4%)	143 (0.1%)	1 (0.6%)
Comorbidities	Hypertension	21,884 (56.8%)	135 (76.7%)	28,308 (23.9%)	61 (38.6%)
	Diabetes	10,312 (26.8%)	39 (22.2%)	15,457 (13.1%)	22 (13.9%)
	Hyperlipidemia	12,267 (31.8%)	70 (39.8%)	21,578 (18.2%)	43 (27.2%)
	Chronic kidney disease	4,896 (12.7%)	14 (8.0%)	10,094 (8.5%)	15 (9.5%)
	Ischemic heart disease	13,686 (35.5%)	30 (17.0%)	12,332 (10.4%)	28 (17.7%)

by calculating Cohen's d between baseline and pre-stroke windows, excluding non-informative metrics ($d \leq 0.05$). Subsequently, to mitigate multicollinearity, we identified variable pairs with high Pearson correlation ($r > 0.80$) and eliminated redundant features. This pipeline resulted in 17 definitive hemodynamic indicators, ensuring that model inputs are both physiologically significant and statistically efficient. The complete nomenclature, definitions, and physiological relevance of these selected biomarkers are detailed in Appendix A.

To transform the continuous hemodynamic streams into a rigorous supervised learning framework, we employed a retrospective labeling protocol anchored to the verified stroke onset time ($t = 0$), as illustrated in Fig. 2. The labeling function $y(t)$ is strictly defined as:

$$y(t) = \begin{cases} 1, & \text{if } -(T_w - \Delta_{pre}) \leq t \leq -\Delta_0 \quad (\text{Warning}) \\ 0, & \text{if } -480 \leq t \leq -(T_w + \Delta_{pre}) \quad (\text{Normal}) \end{cases} \quad (2)$$

To ensure robust decision boundaries, we implemented a dual-exclusion strategy that discards indeterminate samples falling within the transition zones. As depicted by the hatched regions in Fig. 2, the exclusion set $\mathcal{T}_{\text{drop}}$ is defined as:

$$\mathcal{T}_{\text{drop}} = \underbrace{[-(T_w + \Delta_{pre}), -(T_w - \Delta_{pre})]}_{\text{Buffer Time}} \cup \underbrace{(-\Delta_0, 0]}_{\text{Lead Time}} \quad (3)$$

The Buffer Time segregates the stable and pre-stroke phases, mitigating the ambiguity inherent in gradual hemodynamic shifts and preventing boundary overfitting, a strategy compliant with established protocols for indeterminate physiological states [27]. Concurrently, the Lead Time ($\Delta_0 = 15$ min) enforces a strict "blind spot" to preclude feature leakage from imminent events. This 15-minute gap aligns with the minimum intervention window validated in pivotal clinical trials [63], ensuring that predictions rely on latent precursors rather than acute onset artifacts, thereby guaranteeing clinical actionability.

3.5 Predictive Modeling and Evaluation Strategy

We employed a ResNet-1D architecture to capture complex temporal dependencies within the hemodynamic feature space. To effectively mitigate the impact of class imbalance inherent in the dataset, we optimized the network using a Weighted Cross-Entropy Loss with a positive class weight of $\lambda_{\text{pos}} = 3.0$. All models were implemented using the PyTorch framework and trained on an NVIDIA

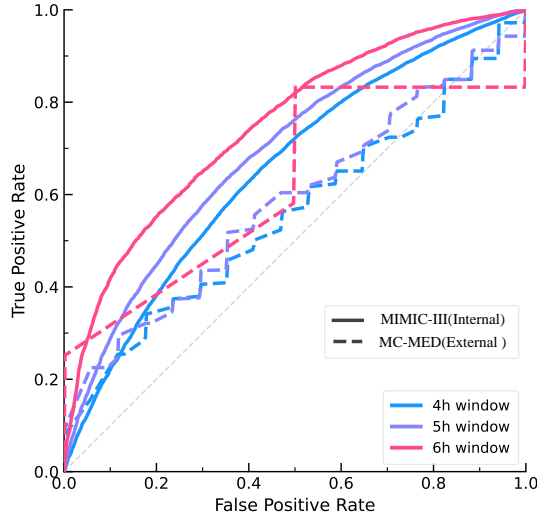


Figure 3: ROC Analysis across internal and external cohorts.
The internal evaluation (solid lines) demonstrates a distinct temporal gradient (6h > 5h > 4h).

RTX 3060 GPU. The training process utilized the Adam optimizer with a learning rate of $\eta = 10^{-3}$ and a weight decay of 10^{-4} to ensure robust and stable convergence.

To ensure patient independence and prevent data leakage, we implemented a stratified patient-level 5-fold cross-validation scheme on the internal MIMIC-III cohort. In this configuration, all data segments associated with a specific patient were confined to a single fold, ensuring that the model is evaluated exclusively on unseen subjects. Validation performance was monitored at each epoch, and the optimal checkpoint was selected based on the maximal Macro F1-score. The final model was subsequently frozen and applied to the external MC-MED cohort for independent testing without further domain adaptation.

4 Experiments and Results

In this section, we evaluate the proposed framework using the internal MIMIC-III cohort for development and the MC-MED cohort for external validation. We analyze the model’s predictive performance across multiple horizons, interrogate the physiological plausibility of learned features, and conduct a rigorous fairness audit across demographic and clinical subgroups.

4.1 Main Predictive Performance

Temporal Window Analysis. We first evaluated the model’s predictive capacity for impending stroke across observation windows of 4, 5, and 6 hours. Results from the internal MIMIC-III cohort (Table 2) reveal a pronounced temporal gradient, where performance maximized at the 6-hour window (AUC 0.7492, F1 0.9406). This trend suggests that extended observation windows facilitate the capture of latent hemodynamic dependencies essential for accurate early warning, transcending a reliance on imminent physiological deterioration. Fig. 3 corroborates this finding across cohorts, demonstrating robust zero-shot generalization to the MC-MED

dataset with consistent monotonic improvement (6h > 5h > 4h). Further statistical decomposition of external performance and label distribution shifts is provided in Section 5.

4.2 Explainable Physiological Insights

We utilized SHAP [36] to verify that predictive power stems from physiological mechanisms rather than artifacts. Fig. 4 reveals consistent pre-stroke signatures across MIMIC-III and MC-MED cohorts driven by a baseline-plus-deviation strategy. Relative Systolic Peak Time $T_{sp,Rel}$ yields the highest positive contribution to log-odds. Its absolute counterpart T_{sp} consistently ranks second. This hierarchy prioritizes patient-specific longitudinal trajectories Rel over static thresholds to isolate acute pathological hardening. The model also integrates hemodynamic instability markers including relative amplitude deviations $A_{sp,Rel}$ and pulse timing variability. The prominence of velocity features like T_o in the external cohort further confirms sensitivity to cardiac ejection efficiency degradation.

We mapped the temporal evolution of high-impact features in Fig. 5 to validate dynamic consistency. A distinct physiological divergence appears in the critical warning zone. The leading predictor, Relative Systolic Peak Time ($T_{sp,Rel}$), exhibits a progressive upward drift. Conversely, absolute Systolic Peak Time (T_{sp}) and stroke volume proxies ($A_{sp,Rel}$) display a synchronized decline. This inverse relationship connects rising systolic timing deviations with dampening hemodynamic force. These patterns confirm that high SHAP scores correspond to tangible pre-stroke decompensation and reinforce clinical validity.

4.3 Stratified Performance Evaluation

We evaluated generalizability using the external MC-MED cohort as depicted in Fig. 6. We assessed whether models trained on the predominantly White MIMIC-III population propagate bias to heterogeneous datasets. The model maintains high utility across racial groups with F1-scores of 0.944 for Black and 0.956 for White cohorts. Performance variances are statistically significant at $p < 0.001$ but absolute scores remain high. The model generalizes to the Asian cohort with an F1-score of 0.921 despite limited training data. This consistency suggests extracted PPG precursors capture physiological features invariant to race. Female patients exhibit slightly higher performance with an F1-score of 0.958 compared to 0.950 for males.

We further examined five comorbidities associated with vascular stiffness defined by specific ICD diagnostic codes. These conditions include Hypertension, Diabetes Mellitus, Hyperlipidemia, Chronic Kidney Disease, and Ischemic Heart Disease. We categorized patients into a Low Risk group with zero comorbidities, a Medium Risk group with one to two, and a High Risk group with three or more. Performance remains strong across strata despite a slight decrease relative to the baseline. F1-scores are 0.968 for Low Risk, 0.943 for Medium Risk, and 0.946 for High Risk groups. F1-scores above 0.94 in complex pathology confirm clinical utility. Performance attenuates in the Elderly cohort aged 65 and older with an F1-score of 0.938 compared to 0.981 in Non-Elderly patients. This significant drop at $p < 0.001$ likely results from arterial stiffness masking hemodynamic signals. High performance confirms effective generalization against vascular aging and chronic comorbidities.

Table 2: Performance comparison of the same ResNet-1D model selection protocol under different early-warning windows on internal (MIMIC) and external (MC-MED) validation cohorts. Results are reported as mean \pm standard deviation over five-fold cross-validation. For each cohort, the best performance across early-warning windows is highlighted in bold.

Window	Dataset	Accuracy	Recall	Precision	F1-score	F2-score	AUC
240 min	MIMIC-III	0.6654 ± 0.0047	0.9833 ± 0.0106	0.6681 ± 0.0041	0.7956 ± 0.0027	0.8985 ± 0.0062	0.6525 ± 0.0530
	MC-MED	0.8636 ± 0.0350	0.9341 ± 0.0413	0.9179 ± 0.0020	0.9256 ± 0.0211	0.9306 ± 0.0332	0.5595 ± 0.1020
300 min	MIMIC-III	0.7860 ± 0.0129	0.9647 ± 0.0360	0.8028 ± 0.0125	0.8759 ± 0.0105	0.9269 ± 0.0243	0.6924 ± 0.0668
	MC-MED	0.9229 ± 0.0273	0.9401 ± 0.0294	0.9802 ± 0.0023	0.9595 ± 0.0151	0.9478 ± 0.0238	0.5847 ± 0.1560
360 min	MIMIC-III	0.8880 ± 0.0028	0.9981 ± 0.0025	0.8894 ± 0.0013	0.9406 ± 0.0015	0.9743 ± 0.0020	0.7492 ± 0.1147
	MC-MED	0.9797 ± 0.0192	0.9804 ± 0.0054	0.9975 ± 0.0008	0.9888 ± 0.0025	0.9837 ± 0.0042	0.7079 ± 0.1248

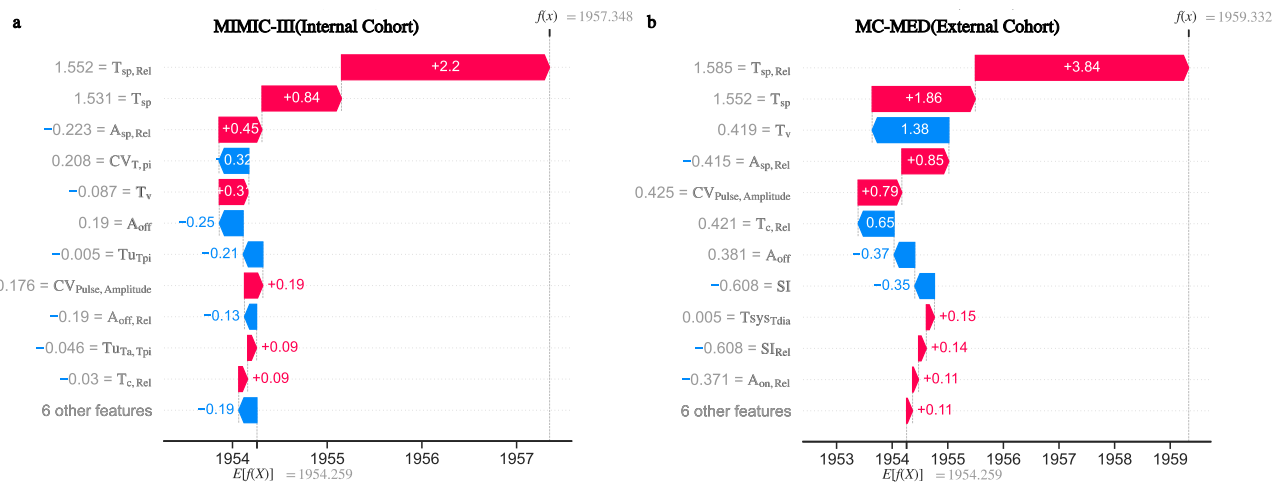


Figure 4: Cross-Dataset SHAP Analysis. Relative Systolic Peak Time ($T_{sp,Rel}$) dominates prediction across cohorts, followed by $CV_{T,p}$ and $A_{sp,Rel}$. (SHAP values scaled by 10^3).

5 Discussion

This study demonstrates that stroke, traditionally regarded as an abrupt and clinically silent event until symptom onset, is preceded by detectable physiological alterations measurable through continuous bedside monitoring. By leveraging PPG signals acquired during routine inpatient care, we show that meaningful hemodynamic signatures emerge several hours before clinically recognized stroke onset. Following are several key clinical discussion points.

Hemodynamic Timing Signatures Preceding In-Hospital Stroke. A key physiological insight from this study is the consistent involvement of two PPG-derived systolic timing features—Systolic Rise Time (SRT) and Time to Maximum Velocity (TMV)—as early indicators of stroke risk. SRT reflects arterial compliance and wave reflection, while TMV, defined by the peak of the first derivative of the PPG waveform, captures early systolic acceleration and ventricular–vascular coupling. SHAP analysis confirms that both features are among the dominant contributors to model predictions across internal and external cohorts, indicating reliance on fundamental hemodynamic mechanisms rather than site-specific artifacts. Their temporal trajectories demonstrate progressive deviation from patient-specific baselines in the hours preceding stroke, suggesting

a gradual loss of systolic efficiency and arterial buffering capacity. From a cardiovascular perspective, these findings imply that stroke onset is preceded by systemic hemodynamic deterioration, in which impaired flow acceleration and altered pulse propagation increase cerebrovascular vulnerability.

Clinical Generalizability and Demographic Equity. To assess clinical generalizability, we evaluated the proposed model across diverse demographics and distributional shifts. The model maintained statistical invariance across multi-ethnic cohorts and various comorbidities (e.g., hypertension, diabetes, and renal disease), suggesting that predictive signatures rely on universal hemodynamic mechanisms rather than demographic artifacts or sensor-induced biases like skin pigmentation. Although geriatric vascular remodeling and arterial stiffness may slightly dampen acute signal detection, individualized baselines preserve clinical efficacy and predictive accuracy. The model demonstrated distributional robustness with superior F1-scores during external validation (Table 2), partially attributable to saturated anomaly ratios (91.31%–99.74%) [15] in the external cohort. This generalization is further corroborated by the consistent discriminative performance maintained across cohorts, confirming the extraction of domain-invariant hemodynamic features.

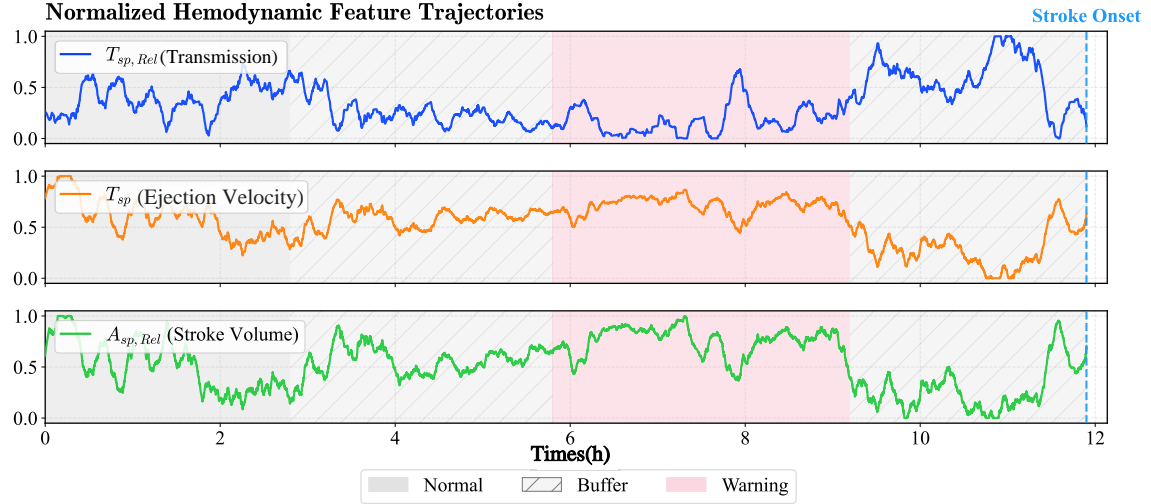


Figure 5: Trajectories of Leading Contributing Factors. Visual validation of the leading contributing factors identified by SHAP. Approaching Stroke Onset, the Relative Systolic Peak Time ($T_{sp, Rel}$) exhibits an upward drift, while the absolute Systolic Peak Time (T_{sp}) and Relative Systolic Amplitude ($A_{sp, Rel}$) show a synchronized downward trend in the final phase. This inverse relationship confirms that the model relies on multidimensional physiological deterioration to predict stroke onset.

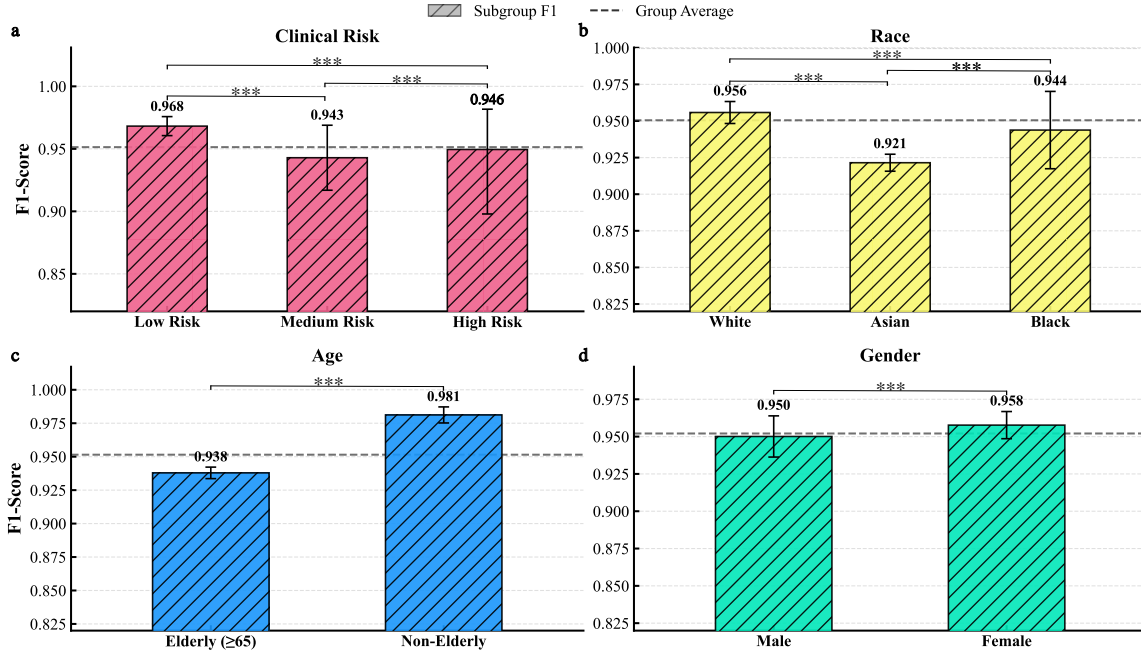


Figure 6: Subgroup performance analysis on the External Cohort (MC-MED). The model demonstrates zero-shot generalization and maintains F1-scores exceeding 0.90 across all racial and clinical subgroups. While performance variances are statistically significant ($p < 0.001$), the consistently high baseline confirms equitable utility despite demographic shifts.

Enabling a Clinically Actionable Pre-Stroke Warning Window. A central clinical implication of this study is the demonstration that stroke may be physiologically detectable several hours before overt neurological deterioration, using signals that are already routinely collected in hospitalized patients. Traditionally,

stroke diagnosis and intervention are triggered only after the appearance of focal neurological deficits, at which point irreversible brain injury may have already occurred. Our findings suggest that continuous PPG monitoring contains hemodynamic signatures that precede clinically recognized stroke by up to six hours, defining a

previously unrecognized pre-onset window that may be amenable to proactive clinical response. From a clinical standpoint, such an early warning signal does not aim to replace neurological examination or imaging-based diagnosis, but rather to function as a risk stratification and surveillance trigger. Patients flagged as high risk could undergo intensified neurological observation, expedited neuroimaging, tighter blood pressure and hemodynamic control, or earlier specialist consultation. Importantly, even modest delays in stroke recognition are known to worsen outcomes; therefore, shifting clinical attention several hours earlier—even without definitive diagnosis—has the potential to materially improve patient trajectories by reducing time-to-intervention once symptoms emerge.

Limitations and Future Work. Despite the robust performance of the framework, several limitations remain. First, the current model lacks the granularity to stratify stroke by subtype, etiology, or severity due to the limited sample size of precisely annotated in-hospital cases. Future research requires larger, prospectively curated datasets to move toward patient-tailored warning systems. Second, while stroke serves as a proof-of-concept, the identified hemodynamic features—such as arterial stiffness and pulse timing—reflect systemic vascular dynamics rather than stroke-specific pathology. This suggests a broad potential for extending this PPG-based framework to other acute conditions involving hemodynamic deterioration, such as sepsis or acute heart failure. Finally, the retrospective nature of this study necessitates prospective validation in real-time clinical workflows to evaluate its actual impact on decision-making and patient outcomes. Integrating these alerts requires a careful balance between diagnostic sensitivity and the practical management of alert burden at the bedside.

6 Conclusion

This work bridges the critical "blind spot" in acute care informatics by introducing an LLM-Enhanced Waveform Anchoring framework, which successfully transforms unstructured clinical narratives into precisely aligned physiological datasets. By unlocking the latent predictive value of continuous PPG signals in confirmed in-hospital stroke cases, our data-centric approach demonstrates that peripheral hemodynamics harbor actionable warning signatures well before onset. Specifically, utilizing a ResNet-1D architecture, the proposed model achieves a clinically significant 6-hour lead time on the internal MIMIC-III cohort with an F1-score of 0.9406 and exhibits remarkable zero-shot generalization to the external MC-MED cohort, attaining an F1-score of 0.9888 without retraining. These findings validate the feasibility of passive, non-invasive monitoring for early stroke detection, marking a pivotal shift from reactive diagnosis to data-driven, proactive prevention in clinical settings.

Generative AI Declaration

This work utilized Gemini 3 Pro (Google) for two specific tasks.

Data Extraction: The model parsed stroke timestamps from unstructured clinical notes. Physicians validated all outputs. See Section 3.2 for the methodology. **Writing Assistance:** The model polished the linguistic flow and grammar. We maintained full editorial control throughout the writing process and take full responsibility for the content.

Acknowledgments

This work was supported in part by the National Natural Science Foundation of China under Grant 62136004, and in part by the National Key R&D Program of China (Grant No. 2023YFF1204803).

References

[1] V. Abedi, V. Avula, D. Chaudhary, S. Shahjouei, A. Khan, C.J. Griessenauer, J. Li, and R. Zand. 2021. Prediction of Long-Term Stroke Recurrence Using Machine Learning Models. *Journal of Clinical Medicine* 10, 6 (2021), 1286. <https://doi.org/10.3390/jcm10061286>

[2] J.N. Acosta, G.J. Falcone, P. Rajpurkar, and E.J. Topol. 2022. Multimodal biomedical AI. *Nature Medicine* 28, 9 (Sep 2022), 1773–1784. <https://doi.org/10.1038/s41591-022-01981-2>

[3] A. Alhakeem, B. Chaurasia, and M.M. Khan. 2025. Revolutionizing stroke prediction: a systematic review of AI-powered wearable technologies for early detection of stroke. *Neurosurgical Review* 48, 1 (May 2025), 458. <https://doi.org/10.1007/s10143-025-03629-4>

[4] A.A. Armondas, S.M. Narayan, D.K. Arnett, K. Spector-Bagdady, D.A. Bennett, L.A. Celi, P.A. Friedman, M.H. Gollob, J.L. Hall, A.E. Kwitek, et al. 2024. Use of Artificial Intelligence in Improving Outcomes in Heart Disease: A Scientific Statement From the American Heart Association. *Circulation* 149, 14 (Apr 2024), e1028–e1050. <https://doi.org/10.1161/CIR.0000000000001201>

[5] Z.I. Attia, D.M. Harmon, E.R. Behr, and P.A. Friedman. 2021. Application of artificial intelligence to the electrocardiogram. *European Heart Journal* 42, 46 (Dec 2021), 4717–4730. <https://doi.org/10.1093/euheartj/ehab649>

[6] K. Bayoumi, M. Gaber, A. Elshafey, O. Mhaimeed, E.H. Dineen, F.A. Marvel, S.S. Martin, E.D. Muse, M.P. Turakhia, K.G. Tarakji, and M.B. Elshazly. 2021. Smart wearable devices in cardiovascular care: where we are and how to move forward. *Nature Reviews Cardiology* 18, 8 (Aug 2021), 581–599. <https://doi.org/10.1038/s41569-021-00522-7>

[7] B. Bent, O.M. Enache, B. Goldstein, W. Kibbe, and J.P. Dunn. 2021. Reply: Matters Arising 'Investigating sources of inaccuracy in wearable optical heart rate sensors'. *npj Digital Medicine* 4, 1 (Feb 2021), 39. <https://doi.org/10.1038/s41746-021-00409-4>

[8] B. Bent, B.A. Goldstein, W.A. Kibbe, and J.P. Dunn. 2020. Investigating sources of inaccuracy in wearable optical heart rate sensors. *npj Digital Medicine* 3, 1 (Feb 2020), 18. <https://doi.org/10.1038/s41746-020-0226-6>

[9] P.H. Charlton, P.A. Kyriaco, J. Mant, V. Marozas, P. Chowienczyk, and J. Alastreuy. 2022. Wearable Photoplethysmography for Cardiovascular Monitoring. *Proceedings of the IEEE* 110, 3 (Mar 2022), 355–381. <https://doi.org/10.1109/JPROC.2022.3149785>

[10] M. Chun, R. Clarke, B.J. Cairns, D.A. Clifton, D. Bennett, Y. Chen, Y. Guo, P. Pei, J. Lv, C. Yu, L. Yang, L. Li, Z. Chen, and T. Zhu. 2021. Stroke risk prediction using machine learning: a prospective cohort study of 0.5 million Chinese adults. *Journal of the American Medical Informatics Association* 28, 8 (2021), 1719–1727. <https://doi.org/10.1093/jamia/ocab068>

[11] GBD 2021 Stroke Risk Factor Collaborators. 2024. Global, regional, and national burden of stroke and its risk factors, 1990–2021: a systematic analysis for the Global Burden of Disease Study 2021. *Lancet Neurology* 23, 10 (Oct 2024), 973–1003. [https://doi.org/10.1016/S1474-4422\(24\)00369-7](https://doi.org/10.1016/S1474-4422(24)00369-7)

[12] E. Dritsas and M. Trigka. 2022. Stroke Risk Prediction with Machine Learning Techniques. *Sensors (Basel)* 22, 13 (Jun 2022), 4670. <https://doi.org/10.3390/s22134670>

[13] J.E. Ebinger and S. Cheng. 2023. From Waveforms to Wisdom: Gleaning More From the ECG About Biological Aging. *Circulation: Cardiovascular Quality and Outcomes* 16, 7 (Jul 2023), e010176. <https://doi.org/10.1161/CIRCOUTCOMES.123.010176>

[14] M. Elgendi, R. Fletcher, Y. Liang, N. Howard, N.H. Lovell, D. Abbott, K. Lim, and R. Ward. 2019. The use of photoplethysmography for assessing hypertension. *NPJ Digital Medicine* 2 (Jun 2019), 60. <https://doi.org/10.1038/s41746-019-0136-7>

[15] Y. Fang, J. Xie, Y. Zhao, L. Chen, Y. Gao, and K. Zheng. 2024. Temporal-Frequency Masked Autoencoders for Time Series Anomaly Detection. In *2024 IEEE 40th International Conference on Data Engineering (ICDE)*. IEEE, Utrecht, Netherlands, 1228–1241.

[16] M. Gadaleta, P. Harrington, E. Barnhill, E. Hytopoulos, M.P. Turakhia, S.R. Steinbuhl, and G. Quer. 2023. Prediction of atrial fibrillation from at-home single-lead ECG signals without arrhythmias. *NPJ Digital Medicine* 6, 1 (Dec 2023), 229. <https://doi.org/10.1038/s41746-023-00966-w>

[17] M.A. Gianfrancesco, S. Tamang, J. Yazdany, and G. Schmajuk. 2018. Potential Biases in Machine Learning Algorithms Using Electronic Health Record Data. *JAMA Internal Medicine* 178, 11 (11 2018), 1544–1547. <https://doi.org/10.1001/jamainternmed.2018.3763>

[18] P.A. Gladding, W. Hewitt, and T.T. Schlegel. 2020. Going Deep With ECG and Aortic Stenosis: Touchdown or Incomplete Pass? *Journal of the American Heart Association* 9, 7 (Apr 2020), e016193. <https://doi.org/10.1161/JAHA.120.016193>

[19] M.A. Goda, P.H. Charlton, and J.A. Behar. 2023. pyPPG: A Python toolbox for comprehensive photoplethysmography signal analysis. *arXiv:2309.13767*

[20] Y. Guo. 2022. A New Paradigm of "Real-Time" Stroke Risk Prediction and Integrated Care Management in the Digital Health Era: Innovations Using Machine Learning and Artificial Intelligence Approaches. *Thrombosis and Haemostasis* 122, 1 (Jan 2022), 5–7. <https://doi.org/10.1055/a-1508-7980>

[21] Y. Guo, H. Wang, H. Zhang, T. Liu, L. Li, L. Liu, M. Chen, Y. Chen, and G.Y.H. Lip. 2021. Photoplethysmography-Based Machine Learning Approaches for Atrial Fibrillation Prediction: A Report From the Huawei Heart Study. *JACC Asia* 1, 3 (Dec 2021), 399–408. <https://doi.org/10.1016/j.jacasi.2021.09.004>

[22] Y. Guo, H. Wang, H. Zhang, T. Liu, Z. Liang, Y. Xia, L. Yan, Y. Xing, H. Shi, S. Li, Y. Liu, F. Liu, M. Feng, Y. Chen, G.Y.H. Lip, and MAFA II Investigators. 2019. Mobile Photoplethysmographic Technology to Detect Atrial Fibrillation. *Journal of the American College of Cardiology* 74, 19 (Nov 2019), 2365–2375. <https://doi.org/10.1016/j.jacc.2019.08.019>

[23] K. He, X. Zhang, S. Ren, and J. Sun. 2016. Deep Residual Learning for Image Recognition. In *2016 IEEE Conference on Computer Vision and Pattern Recognition (CVPR 2016), Las Vegas, NV, USA, June 27–30, 2016*. IEEE Computer Society, Las Vegas, NV, USA, 770–778. <https://doi.org/10.1109/CVPR.2016.90>

[24] J. Heo, J. Yoo, H. Lee, I.H. Lee, J.S. Kim, E. Park, Y.D. Kim, and H.S. Nam. 2022. Prediction of Hidden Coronary Artery Disease Using Machine Learning in Patients With Acute Ischemic Stroke. *Neurology* 99, 1 (Jul 2022), e55–e65. <https://doi.org/10.1212/WNL.00000000000020576>

[25] H.Y. Ho, K.Y. Liang, W.C. Lin, S. Kitanaka, and J.B. Wu. 2010. Regulation and improvement of triterpene formation in plant cultured cells of *Eriobotrya japonica* Lindl. *Journal of Bioscience and Bioengineering* 110, 5 (Nov 2010), 588–592. <https://doi.org/10.1016/j.jbi.2010.06.009>

[26] A. Hughes, M.M.H. Shandhi, H. Master, J. Dunn, and E. Brittain. 2023. Wearable Devices in Cardiovascular Medicine. *Circulation Research* 132, 5 (Mar 2023), 652–670. <https://doi.org/10.1161/CIRCRESAHA.122.322389>

[27] S.L. Hyland, M. Faltys, M. Hüser, X. Lyu, T. Gumbusch, C. Esteban, C. Bock, M. Horn, M. Moor, B. Rieck, M. Zimmermann, D. Bodenham, K. Borgwardt, G. Rätsch, and T.M. Merz. 2020. Early prediction of circulatory failure in the intensive care unit using machine learning. *Nature Medicine* 26, 3 (2020), 364–373. <https://doi.org/10.1038/s41591-020-0789-4>

[28] Y. Jin, C. Qin, Y. Huang, W. Zhao, and C. Liu. 2020. Multi-domain modeling of atrial fibrillation detection with twin attentional convolutional long short-term memory neural networks. *Knowledge-Based Systems* 193 (2020), 105460. <https://doi.org/10.1016/j.knosys.2019.105460>

[29] A. Kansal, E. Chen, T. Jin, P. Rajpurkar, and D. Kim. 2025. Multimodal Clinical Monitoring in the Emergency Department (MC-MED). *PhysioNet*. <https://doi.org/10.13026/jz99-4j81> Version 1.0.0.

[30] S. Khurshid, S. Friedman, C. Reeder, P. Di Achille, N. Diamant, P. Singh, L.X. Harrington, X. Wang, M.A. Al-Asli, G. Sarma, A.S. Foulkes, P.T. Ellinor, C.D. Anderson, J.E. Ho, A.A. Philippakis, P. Batra, and S.A. Lubitz. 2022. ECG-Based Deep Learning and Clinical Risk Factors to Predict Atrial Fibrillation. *Circulation* 145, 2 (Jan 2022), 122–133. <https://doi.org/10.1161/CIRCULATIONAHA.121.057480>

[31] D.O. Kleindorfer, A. Towfighi, S. Chaturvedi, K.M. Cockroft, J. Gutierrez, D. Lombardi-Hill, H. Kamel, W.N. Kernan, S.J. Kittner, E.C. Leira, O. Lennon, J.F. Meschia, T.N. Nguyen, P.M. Pollak, S. Santangeli, A.Z. Sharrief, S.C. Smith Jr., T.N. Turan, and L.S. Williams. 2021. 2021 Guideline for the Prevention of Stroke in Patients With Stroke and Transient Ischemic Attack: A Guideline From the American Heart Association/American Stroke Association. *Stroke* 52, 7 (Jul 2021), e364–e467. <https://doi.org/10.1161/STR.000000000000375>

[32] D. Kumar, A. Peimankar, K. Sharma, H. Domínguez, S. Puthusserypady, and J.E. Bardram. 2022. Deepaware: A hybrid deep learning and context-aware heuristics-based model for atrial fibrillation detection. *Computers in Methods and Programs in Biomedicine* 221 (Jun 2022), 106899. <https://doi.org/10.1016/j.cmpb.2022.106899>

[33] Y. Li, H. Godwin, M. Cecelja, K. O'Gallagher, A. Shah, A. Douiri, and P. Chowienczyk. 2025. Prediction of Cardiovascular Disease Events From the Photoplethysmograph Waveform. *Journal of the American Heart Association* 14, 24 (Dec 2025), e040237. <https://doi.org/10.1161/JAHA.124.040237>

[34] G.Y.H. Lip, A. Genaidy, G. Tran, P. Marroquin, C. Estes, and S. Sloop. 2022. Improving Stroke Risk Prediction in the General Population: A Comparative Assessment of Common Clinical Rules, a New Multimorbid Index, and Machine-Learning-Based Algorithms. *Thrombosis and Haemostasis* 122, 1 (Jan 2022), 142–150. <https://doi.org/10.1055/a-1467-2993>

[35] S.A. Lubitz, A.Z. Faranesh, C. Selvaggi, S.J. Atlas, D.D. McManus, D.E. Singer, S. Pagoto, M.W. McConnell, A. Pantelopoulos, and A.S. Foulkes. 2022. Detection of Atrial Fibrillation in a Large Population Using Wearable Devices: The Fitbit Heart Study. *Circulation* 146, 19 (Nov 2022), 1415–1424. <https://doi.org/10.1161/CIRCULATIONAHA.122.060291>

[36] S.M. Lundberg and S.-I. Lee. 2017. A Unified Approach to Interpreting Model Predictions. In *Advances in Neural Information Processing Systems*, I. Guyon, U. Von Luxburg, S. Bengio, H. Wallach, R. Fergus, S. Vishwanathan, and R. Garnett (Eds.), Vol. 30. Curran Associates, Inc., Long Beach, CA, USA.

[37] M.E. Matheny, I. Ricket, C.A. Goodrich, R.U. Shah, M.E. Stabler, A.M. Perkins, C. Dorn, J. Denton, B.E. Bray, R. Gouripeddi, J. Higgins, W.W. Chapman, T.A. MacKenzie, and J.R. Brown. 2021. Development of Electronic Health Record-Based Prediction Models for 30-Day Readmission Risk Among Patients Hospitalized for Acute Myocardial Infarction. *JAMA Network Open* 4, 1 (Jan 2021), e2035782. <https://doi.org/10.1001/jamanetworkopen.2020.35782>

[38] A.C. Miller, J. Futoma, S. Abbaspourazad, C. Heinze-Deml, S. Emrani, I. Shapiro, and G. Sapiro. 2025. A wearable-based aging clock associates with disease and behavior. *Nature Communications* 16, 1 (Oct 2025), 9264. <https://doi.org/10.1038/s41467-025-64275-4>

[39] A. Mincholé and B. Rodriguez. 2019. Artificial intelligence for the electrocardiogram. *Nature Medicine* 25, 1 (Jan 2019), 22–23. <https://doi.org/10.1038/s41591-018-0306-1>

[40] B. Moody, G. Moody, M. Villarreal, G.D. Clifford, and I. Silva. 2020. MIMIC-III Waveform Database Matched Subset. PhysioNet. <https://doi.org/10.13026/c2294b> Version 1.0.

[41] M. Moor, O. Banerjee, Z.S.H. Abad, H.M. Krumholz, J. Leskovec, E.J. Topol, and P. Rajpurkar. 2023. Foundation models for generalist medical artificial intelligence. *Nature* 616, 7956 (Apr 2023), 259–265. <https://doi.org/10.1038/s41586-023-05881-4>

[42] R. Mukkamala, G.S. Stergiou, and A.P. Avolio. 2022. Cuffless Blood Pressure Measurement. *Annual Review of Biomedical Engineering* 24 (Jun 2022), 203–230. <https://doi.org/10.1146/annurev-bioeng-110220-014644>

[43] G. Nie, Q. Zhao, G. Tang, Y. Li, and S. Hong. 2025. Artificial intelligence-derived photoplethysmography age as a digital biomarker for cardiovascular health. *Communications Medicine* 5, 1 (Nov 2025), 481. <https://doi.org/10.1038/s43856-025-01188-9>

[44] T. Pereira, N. Tran, K. Gadhoumi, M.M. Pelter, D.H. Do, R.J. Lee, R. Colorado, K. Meisel, and X. Hu. 2020. Photoplethysmography based atrial fibrillation detection: a review. *NPJ Digital Medicine* 3 (Jan 2020), 3. <https://doi.org/10.1038/s41746-019-0207-9>

[45] G. Petmezias, K. Haris, L. Stefanopoulos, V. Kilintzis, A. Tzavelis, J.A. Rogers, A.K. Katsaggelos, and N. Maglaveras. 2021. Automated Atrial Fibrillation Detection using a Hybrid CNN-LSTM Network on Imbalanced ECG Datasets. *Biomedical Signal Processing and Control* 63 (2021), 102194. <https://doi.org/10.1016/J.BSPC.2020.102194>

[46] X. Qin, S. Yi, J. Rong, H. Lu, B. Ji, W. Zhang, R. Ding, L. Wu, and Z. Chen. 2023. Identification of anoikis-related genes classification patterns and immune infiltration characterization in ischemic stroke based on machine learning. *Frontiers in Aging Neuroscience* 15 (Mar 2023), 1142163. <https://doi.org/10.3389/fnagi.2023.1142163>

[47] G. Quer, J.M. Radin, M. Gadaleta, K. Baca-Motes, L. Ariniello, E. Ramos, V. Kheterpal, E.J. Topol, and S.R. Steinhubl. 2021. Wearable sensor data and self-reported symptoms for COVID-19 detection. *Nature Medicine* 27, 1 (Jan 2021), 73–77. <https://doi.org/10.1038/s41591-020-1123-x>

[48] S. Raghunath, A.E. Ulloa Cerna, L. Jing, D.P. vanMaanen, J. Stough, D.N. Hartzel, J.B. Leader, H.L. Kirchner, M.C. Stumpf, A. Hafez, A. Nemani, T. Carbonati, K.W. Johnson, K. Young, C.W. Good, J.M. Pfeifer, A.A. Patel, B.P. Delisle, A. Alsaid, D. Beer, C.M. Haggerty, and B.K. Fornwalt. 2020. Prediction of mortality from 12-lead electrocardiograms voltage data using a deep neural network. *Nature Medicine* 26, 6 (Jun 2020), 886–891. <https://doi.org/10.1038/s41591-020-0870-z>

[49] L. Rasmay, Y. Xiang, Z. Xie, C. Tao, and D. Zhi. 2021. Med-BERT: pretrained contextualized embeddings on large-scale structured electronic health records for disease prediction. *NPJ Digital Medicine* 4, 1 (May 2021), 86. <https://doi.org/10.1038/s41746-021-00455-y>

[50] A.H. Ribeiro, M.H. Ribeiro, G.M.M. Paixão, D.M. Oliveira, P.R. Gomes, J.A. Canazart, M.P.S. Ferreira, C.R. Andersson, P.W. Macfarlane, W. Meira Jr, T.B. Schön, and A.L.P. Ribeiro. 2020. Author Correction: Automatic diagnosis of the 12-lead ECG using a deep neural network. *Nature Communications* 11, 1 (May 2020), 2227. <https://doi.org/10.1038/s41467-020-16172-1>

[51] N. Sambasivan, S. Kapania, H. Highfill, D. Akrong, P.K. Paritosh, and L. Aroyo. 2021. "Everyone wants to do the model work, not the data work": Data Cascades in High-Stakes AI. In *CHI '21: CHI Conference on Human Factors in Computing Systems, Virtual Event / Yokohama, Japan, May 8-13, 2021*. ACM, New York, NY, USA, 39:1–39:15. <https://doi.org/10.1145/341764.3445518>

[52] L.I. Santos, M.O. Camargos, M.F.S.V. D'Angelo, J.B. Mendes, E.E.C. de Medeiros, A.L.S. Guimarães, and R.M. Palhares. 2022. Decision tree and artificial immune systems for stroke prediction in imbalanced data. *Expert Systems with Applications* 191 (2022), 116221. <https://doi.org/10.1016/j.eswa.2021.116221>

[53] K.C. Sontios, P.A. Noseworthy, A. Arghami, S.A. Weston, Z.I. Attia, J.A. Crestanello, P.A. Friedman, A.M. Chamberlain, and B.J. Gersh. 2021. Use of Artificial Intelligence Tools Across Different Clinical Settings: A Cautionary Tale. *Circulation: Cardiovascular Quality and Outcomes* 14, 9 (Sep 2021), e008153. <https://doi.org/10.1161/CIRCOUTCOMES.121.008153>

[54] M.S. Sirsat, E. Fermé, and J. Câmara. 2020. Machine Learning for Brain Stroke: A Review. *Journal of Stroke and Cerebrovascular Diseases* 29, 10 (2020), 105162. <https://doi.org/10.1016/j.jstrokecerebrovasdis.2020.105162>

[55] N. Strodtthoff, P. Wagner, T. Schaeffter, and W. Samrek. 2021. Deep Learning for ECG Analysis: Benchmarks and Insights from PTB-XL. *IEEE Journal of Biomedical and Health Informatics* 25, 5 (May 2021), 1519–1528. <https://doi.org/10.1109/JBHI.2020.3022989>

[56] E. Svensson, L. Friberg, V. Frykman, F. Al-Khalili, J. Engdahl, and M. Rosenqvist. 2021. Clinical outcomes in systematic screening for atrial fibrillation (STROKESTOP): a multicentre, parallel group, unmasked, randomised controlled trial. *The Lancet* 398, 10310 (Oct 2021), 1498–1506. [https://doi.org/10.1016/S0140-6736\(21\)01637-8](https://doi.org/10.1016/S0140-6736(21)01637-8)

[57] A.J. Thirunavukarasu, D.S.J. Ting, K. Elangovan, L. Gutierrez, T.F. Tan, and D.S.W. Ting. 2023. Large language models in medicine. *Nature Medicine* 29, 8 (Aug 2023), 1930–1940. <https://doi.org/10.1038/s41591-023-02448-8>

[58] H.A. Tzou, S.F. Lin, and P.S. Chen. 2021. Paroxysmal atrial fibrillation prediction based on morphological variant P-wave analysis with wideband ECG and deep learning. *Computers in Methods and Programs in Biomedicine* 211 (Nov 2021), 106396. <https://doi.org/10.1016/j.cmpb.2021.106396>

[59] US Preventive Services Task Force, K.W. Davidson, M.J. Barry, C.M. Mangione, M. Cabana, A.B. Caughey, E.M. Davis, K.E. Donahue, C.A. Doubeni, J.W. Epling Jr, M. Kubik, L. Li, G. Ogedegbe, L. Pbert, M. Silverstein, J. Stevermer, C.W. Tseng, and J.B. Wong. 2022. Screening for Atrial Fibrillation: US Preventive Services Task Force Recommendation Statement. *JAMA* 327, 4 (Jan 2022), 360–367. <https://doi.org/10.1001/jama.2021.23732>

[60] A. Vodencarevic, M. Weingärtner, J.J. Caro, D. Ukalovic, M. Zimmermann-Ritterreiser, S. Schwab, and P. Kolominsky-Rabas. 2022. Prediction of Recurrent Ischemic Stroke Using Registry Data and Machine Learning Methods: The Erlangen Stroke Registry. *Stroke* 53, 7 (Jul 2022), 2299–2306. <https://doi.org/10.1161/STROKEAHA.121.036557>

[61] C. Wang, B. Qi, M. Lin, Z. Zhang, M. Makihata, B. Liu, S. Zhou, Y.H. Huang, H. Hu, Y. Gu, Y. Chen, Y. Lei, T. Lee, S. Chien, K.I. Jang, E.B. Kistler, and S. Xu. 2021. Continuous monitoring of deep-tissue haemodynamics with stretchable ultrasonic phased arrays. *Nature Biomedical Engineering* 5, 7 (Jul 2021), 749–758. <https://doi.org/10.1038/s41551-021-00763-4>

[62] W.H. Weng, S. Baur, M. Daswani, C. Chen, L. Harrell, S. Kakarmath, M. Jabara, B. Behsaz, C.Y. McLean, Y. Matias, G.S. Corrado, S. Shetty, S. Prabhakara, Y. Liu, G. Danaei, and D. Ardia. 2024. Predicting cardiovascular disease risk using photoplethysmography and deep learning. *PLOS Global Public Health* 4, 6 (Jun 2024), e0003204. <https://doi.org/10.1371/journal.pgph.0003204>

[63] M. Wijnberge, B.F. Geerts, L. Hol, N. Lemmers, M.P. Mulder, P. Berge, J. Schenck, J. van der Hoeven, J.J. Vos, G. Scheffer, et al. 2020. Effect of a machine learning-derived early warning system for intraoperative hypotension vs standard care on depth and duration of hypotension during elective noncardiac surgery: the HYPE randomized clinical trial. *JAMA* 323, 11 (2020), 1052–1060. <https://doi.org/10.1001/jama.2020.0592>

[64] E. Yang, A.E. Schutte, G. Stergiou, F.S. Wyss, Y. Commodore-Mensah, A. Odili, I. Kronish, H.Y. Lee, and D. Shimbo. 2025. Cuffless Blood Pressure Measurement Devices—International Perspectives on Accuracy and Clinical Use: A Narrative Review. *JAMA Cardiology* 10, 6 (Jun 2025), 624–631. <https://doi.org/10.1001/jamacardio.2025.0662>

[65] P. Zhang, Y. Chen, F. Lin, S. Wu, X. Yang, and Q. Li. 2022. Semi-Supervised Learning for Automatic Atrial Fibrillation Detection in 24-Hour Holter Monitoring. *IEEE Journal of Biomedical and Health Informatics* 26, 8 (Aug 2022), 3791–3801. <https://doi.org/10.1109/JBHI.2022.3173655>

A Hemodynamic Feature Definitions

Table 3 provides a comprehensive reference for the 17 hemodynamic features extracted in this study. To facilitate interpretation, biomarkers are categorized into four groups: (I) Time-Domain & Morphological features representing the structural characteristics of a single cardiac cycle; (II) Derivative & Normalized features reflecting internal flow dynamics; (III) Short-Term Variability features quantifying autonomic regulation; and (IV) Relative Deviation features capturing the kinematic trajectory of pathological evolution relative to the patient's baseline.

Table 3: Detailed Definitions and Physiological Significance of Hemodynamic Features. Features are derived from the raw PPG signal, Velocity Plethysmogram (VPG), and Acceleration Plethysmogram (APG).

Symbol	Definition	Physiological Significance
<i>I. Time-Domain & Morphological Features (Structural Basis)</i>		
T_{sp}	Time to Systolic Peak: Time elapsed from pulse onset to the systolic peak.	Reflects velocity of blood ejection and wave transmission. Related to arterial compliance; typically shortens with stiffening.
SI	Stiffness Index: Ratio of pulse amplitude to systolic time (T_{sys}).	Represents average slope of systolic upstroke. Higher index indicates increased arterial stiffness (vascular aging proxy).
A_{off}	Offset Amplitude: Signal amplitude at the pulse offset point.	Reflects vascular recoil at end-diastole, correlating with vessel elasticity and venous return.
T_{sys}/T_{dia}	Systolic-Diastolic Ratio: Ratio of systolic duration to diastolic duration.	Describes temporal balance of cardiac cycle. Imbalances indicate autonomic dysfunction or abnormal resistance.
<i>II. Derivative & Normalized Features (Internal Dynamics)</i>		
$T_{u_{Tp_i}}$	Norm. Time to VPG Peak: Time to max velocity (u-wave) normalized by pulse interval (T_{pi}).	Reflects relative duration of rapid ejection phase. Associated with vascular impedance and flow inertia.
$T_{b_{Tp_i}}$	Norm. Time to APG b-wave: Time to b-wave in 2nd derivative normalized by T_{pi} .	Sensitive to vascular aging and augmentation of peripheral reflection waves (early hardening).
T_v	Time to VPG Valley: Time to VPG inflection point (v-wave) post-systole.	Correlates with timing of reflected wave return; reflects coupling of central and peripheral hemodynamics.
$T_{u_{Ta,Tpi}}$	VPG-APG Peak Delay Ratio: Temporal difference between peak velocity and acceleration.	Describes decoupling between peak velocity and acceleration. Sensitive marker for neurovascular mismatch.
<i>III. Short-Term Variability Features (Autonomic Regulation)</i>		
$CV_{T_{pi}}$	Pulse Interval Variability: Coefficient of Variation (CV) of the pulse interval.	Surrogate for ultra-short-term HRV. Reductions indicate autonomic imbalance and loss of vagal tone.
CV_{PA}	Amplitude Variability: Coefficient of Variation of pulse amplitudes.	Reflects sympathetic capacity to modulate peripheral tone. Reduced variability suggests rigid regulation.
<i>IV. Relative Deviation Features (Pathological Evolution)</i>		
$T_{sp,Rel}$	Relative T_{sp}: Deviation of current T_{sp} from individual baseline.	Captures progressive drift in wave transmission time, robust to inter-subject baseline variability.
$A_{sp,Rel}$	Relative Systolic Amplitude: Deviation of systolic peak magnitude.	Highly sensitive to acute changes in vascular compliance and stroke volume prior to event.
SI_{Rel}	Relative Stiffness Index: Deviation of the Stiffness Index from baseline.	Tracks trajectory of arterial hardening (compliance degradation) leading up to stroke.
DSI_{Rel}	Relative Dynamic Stability: Deviation of the Dynamic Stability Index from baseline.	Quantifies shift in morphological proportions. Indicator of "loss of homeostasis" in hemodynamic system.
$T_{c,Rel}$	Relative APG c-wave: Shift in the late-systolic c-wave timing.	Relates to late-systolic recoil; reveals acute abnormalities in arterial wall elasticity.
$A_{off,Rel}$	Relative Offset Amp: Deviation in end-diastolic amplitude.	Associated with shifts in venous return and diastolic regulation efficiency.
$A_{on,Rel}$	Relative Onset Amp: Deviation in pulse onset nadir.	Sensitive to perfusion abnormalities in peripheral microcirculation.